mater.scichina.com link.springer.com

Published online 9 December 2022 | https://doi.org/10.1007/s40843-022-2282-9
Sci China Mater 2023, 66(4): 1607–1614

Self-cleaning solar water evaporation device based on polyaniline/TiO_2/natural cellulose fibers for contaminant water

Wenning Liu, Pengfei Li, Xiangqin Li, Yaqian He, Li An, Dan Qu, Xiayan Wang and Zaicheng Sun*

ABSTRACT **Wastewater accounts for a large part of the water body on the earth. Solar water evaporation is an effective way to produce fresh water from seawater or polluted water. However, the co-evaporation or deposition of contaminants may reduce the efficiency and freshwater quality during water evaporation. In this work, a self-cleaning solar water evaporator is developed based on the natural lignocellulose fibers (NCF), polyaniline (PANI), and TiO_2, which shows great advantages of wide-range light absorption, super hydrophilicity, and low thermal conductivity. Nanofibrous PANI is polymerized on the surface of NCF to form a mesoporous network by adding the NCF to the polymerization solution. P25 TiO_2 nanoparticles as photocatalysts are dispersed into the above reaction to form the hybrid PANI/TiO_2/NCF composite disc by simply filtration. Owing to the synergistic effect between the photothermal PANI and the photocatalytic degradation of TiO_2 nanoparticles in the solar water evaporator device, the water evaporation rate can reach 2.36 kg m^{-2} h^{-1} (under 1 sun irradiation), and the contaminant (100 ppm tetracycline) can be efficiently degraded. Interestingly, the solar water evaporator device still maintains a constant solar evaporation rate after working for 10 h, and no contaminant is accumulated. The bifunctional solar water evaporation device, which combines photocatalytic and photothermal effects, has great potential application in organic contaminant water with a self-cleaning effect.**

Keywords: self-cleaning, solar water evaporation, photocatalytic, contaminant water

INTRODUCTION

Less than 1% of all the freshwater stored in the atmosphere, rivers, lakes, and underground has to support the Earth's population. Increasing pollution of the rivers and lakes has caused a serious freshwater crisis. The shortage of fresh water is becoming a threat to the sustainable development of human society [1]. Organic compounds and antibiotics are often detected in sediments [2], landfills [3], lakes and rivers [4], drinking water sources [5], and groundwater [6] due to their over-use in aquaculture farming and livestock breeding. Long-term exposure to low levels of residual antibiotics may lead to super bacteria with drug resistance [7]. Antibiotic contaminants have become a serious threat to public health and the social environment. As a result, it is of great significance to develop efficient and economical treatment technology to obtain drinkable water from contaminant water [8].

Solar water evaporation, based on renewable clean solar energy, is one of the most promising methods to produce clean water from seawater or sewage to alleviate the freshwater crisis [9–12]. The traditional solar water evaporation approaches not only have poor solar energy absorption, but also low light–heat conversion efficiency due to the fact that the light absorbent is placed at the bottom of the bulk water [13,14]. In the interface solar evaporation systems, the light absorber is placed at the water-air interface so that the water-air interface is heated instead of bulk water, which greatly improves the solar water evaporation efficiency [15–21]. As an ideal solar evaporator, it has several key features: an efficient collection of solar energy, low heat transfer coefficient, reduced heat loss, good hydrophilicity, and a porous frame to accelerate steam escape. Photothermal materials convert absorbed light into heat through thermalization and nonradiative recombination of photoexcited electron-hole pairs [10]. The development of broadband photothermal absorbing materials provides an effective strategy for the efficient use of solar energy to produce fresh water. So far, it is reported that several materials with broad and powerful solar energy absorption characteristics and stable energy conversion performance, including semiconductor materials [22], metal nanoparticles [23–25], carbon-based materials [26,27], and polymer materials [28–30], have been used for solar desalination. At present, photothermal materials used in solar evaporators are mainly metallic nanoparticles, semiconductor materials, and carbon-based materials [31]. Polymer materials have attracted extensive attention in the manufacture of high-performance solar absorbers because of the advantages of easy process, high photothermal conversion efficiency, low cost, durability, and lightweight [32–34]. However, the current choice of polymers is limited [35], and the development of suitable polymer materials and nanostructures is particularly important for solar water evaporation. A hydrophilic and porous framework ensures good water transportation and a large interfacial surface of water-air for evaporation. However, to produce fresh water from contaminant water or seawater, the contaminant's co-evaporation or deposition may reduce the device efficiency and the quality of the freshwater during the purification of the polluted water. Self-cleaning solar water evaporation device is an ideal model for freshwater production.

Antibiotics have been a serious contaminant for the common waterbody. Photocatalytic degradation of antibiotics is considered to be one of the most promising methods because of its advantages of fast operation, low cost, and high efficiency.

Center of Excellence for Environmental Safety and Biological Effects, Beijing Key Laboratory for Green Catalysis and Separation, Faculty of Environment and Life, Beijing University of Technology, Beijing 100124, China

Photocatalytic degradation can degrade antibiotic pollutants without causing secondary pollution [36,37]. As a promising photocatalyst, TiO_2 has attracted extensive attention in many photocatalysis areas because of its advantages of nontoxicity, low cost, physicochemical stability, and easy production [38]. The combination of photothermal materials and photo-catalysts is an effective route to produce high-quality water and remove contaminants at the same time.

Li *et al.* [39] prepared multifunctional cotton fabrics (polyaniline (PANI)/Ag/multi-walled carbon nanotubes-COOH/polydopamine@biochemical cotton) with the functions of organic pollution treatment and water evaporation by *in-situ* chemical polymerization technology, and the water evaporation rate reached 1.37 kg m^{-2} h^{-1} under 1 sun illumination. Hao *et al.* [29] proposed a multifunctional cotton fabric with photothermal and photocatalytic properties prepared by *in-situ* polymerization of pyrrole on cotton and then depositing TiO_2 nanoparticles, which achieved a high solar water evaporation rate (1.55 kg m^{-2} h^{-1} under 1 sun illumination) and efficient photocatalytic degradation of methyl orange (96%). Xing *et al.* [28] reported a high-efficiency ammonia responsive solar evaporator based on TiO_2 nanoparticles and polypyrrole nanoparticles. The water evaporation rate of the solar evaporator can reach 2.9 kg m^{-2} h^{-1} under 2 sun illumination, and it can effectively degrade organic pollutants. The morphology of the polymer limits its photothermal conversion efficiency. PANI is a conductive polymer with a wide absorption range, and nanofibrous morphology is achieved by simple chemical oxidation polymerization [40,41]. The hybrid of PANI and TiO_2 nanoparticles can improve light absorption and promote photocatalytic degradation of organic contaminants [37].

Herein, we propose a bifunctional solar water evaporator that combines photothermal and photocatalytic degradation to obtain fresh water from organic wastewater. To construct a high-efficiency solar water evaporator, a hydrophilic porous structure is created by natural lignocellulose fiber (NCF). PANI nanofibers are grown on cellulose fiber by the *in-situ* polymerization with the presence of NCF according to the previous report [42]. P25 TiO_2 nanoparticles are dispersed to the polymerization reaction to achieve the hybrid TiO_2/PANI/NCF. The two-dimensional (2D) evaporator device is fabricated by simple filtration. NCF has a relatively low thermal conductivity of 0.0617 W m^{-1} k^{-1} [43]. PANI nanofibers exhibit excellent light absorption covering the whole solar spectrum and photothermal conversion properties. TiO_2 as a typical photocatalyst can efficiently degrade the organic contaminant. Overall, the solar water evaporator presents an excellent water evaporation rate of 2.36 kg m^{-2} h^{-1} (under 1 sun irradiation) and complete degradation of tetracycline (TC).

EXPERIMENTAL SECTION

Chemicals and materials

Hydrochloric acid (37%), aniline (≥99.5%), ammonium persulfate (99.99%, APS), titanium dioxide (Degussa P25 TiO_2 with an average particle size of 25 nm), TC (≥98%), sodium chloride (AR), and medium-speed qualitative filter paper as NCF were used as-received in all experiments.

Preparation of PANI/NCF

APS (0.96 g, 4 mmol) was dissolved in 100 mL of HCl (1.0 mol L^{-1}) and cooled down to about 0°C, and it was denoted as solution A. NCF (1.28 g) was added to 100 mL of HCl under mild stirring till to forming a pulp. Aniline (1.6 mL, ~17 mmol) was added to the above pulp dispersion and cooled down to 0°C, and it was named solution B. The above two solutions were mixed, and stirred dramatically for a few minutes, and then the reaction was left in the 0°C refrigerators overnight. PANI nanofibers were synthesized on the surface of NCF to form a secondary structure of the two fibers. After the reaction, the solution was filtered, washed with deionized (DI) water to neutral, and dried to obtain PANI/NCF disc for solar water evaporation.

Preparation of PANI/TiO_2/NCF composites

A similar procedure was employed to prepare the bifunctional solar water evaporator device by adding different amounts of TiO_2 into the reaction solution B. The molar ratio of APS/aniline was set as 1:4. Different amounts of TiO_2 (0–1 g) and NCF (0.32–2.56 g) were added to the reaction to optimize the photocatalytic activity and device thickness.

Experimental setup for water evaporation

Water and TC solution (100 ppm) were placed in a 25-mL beaker. The solar water evaporation device was fabricated according to our previous report [44]. The PANI/NCF or PANI/TiO_2/NCF was mechanically combined with the suede in a disc shape. To prevent light irradiation and heat conduction, a piece of polystyrene foam (9 cm × 9 cm × 1 cm) was placed between the beaker and the device. The whole system was placed on an electronic analytical balance with a resolution of 0.1 mg to monitor the mass change during the water evaporation under 1 sun illumination after stabilization for 30 min. The control sample was obtained by carrying out the above setup under dark conditions. The evaporation rates were obtained by subtracting the evaporation rate of water under dark from that under light irradiation.

Photocatalytic degradation evaluation

Ultraviolet-visible (UV-vis) spectroscopy was used to determine the TC concentration based on the calibration curve. PANI/NCF and PANI/TiO_2/NCF discs were placed in two identical beakers containing 100 ppm TC solution for overnight to reach adsorption saturation under dark conditions, respectively. The discs were taken out and soaked in the same volume of DI water to reach the balance of the adsorption-desorption to remove free TC from the disc. The mass of TC (M_{B0}) released from the device can be obtained from the concentration of TC based on the UV-vis absorption intensity. This device was further used for water evaporation for 10 h. The base solution (the liquid in the beaker) was 100 ppm TC solution. During water evaporation, TC was transferred to the disc by water and accumulated on the disc with the water evaporation. The TC adsorption saturated disc was used for solar water evaporation. Then, all the TC should be deposited on the disc during the water evaporation. After that, the discs were removed from the device and put into the same volume of DI water overnight to reach the balance of the adsorption-desorption. After that, the device was immersed in DI water to release the free TC (M_{L0}). The M_{L0} including M_{B0} and deposited TC during water evaporation (M_0) can be calculated from $M_0 = M_{L0} - M_{B0}$ based on the UV-vis absorption intensity. Similarly, M_X can be obtained for the PANI/TiO_2/NCF

samples, where X stands for different TiO_2 amounts (0–1 g) in the device. The difference ($M_0 - M_X$) is the amount of TC which is degraded by photocatalyst.

RESULTS AND DISCUSSION

Characterization of the bifunctional solar water evaporator

Fig. S1a exhibits the scanning electron microscopy (SEM) image of NCF with a smooth surface and micrometer scale in diameter. PANI nanowires can be easily synthesized by static polymerization according to previous report [42]. Fig. S1b displays SEM images of PANI nanowires from static polymerization. The PANI nanowires exhibit a uniform diameter of 50 nm. PANI/NCF composites can be achieved by adding NCF into the polymerization solution of aniline. The PANI/NCF fibrous disc was fabricated by simply filtration of the polymerization dispersion and then washing with DI water and drying in the oven. Fig. 1a presents the SEM image of PANI/NCF composites with both microfiber and nanofiber morphologies. The microfibers are NCF and the nanofibers are PANI. To fabricate the bifunctional PANI/TiO_2/NCF fibrous disc, P25 TiO_2 was added to the polymerization solution except for NCF. The TiO_2 nanoparticles mixed with PANI nanofibers cover the NCF (Fig. 1b, c).

To further verify the composition of the composite fiber network, the samples were characterized by Fourier transformed infrared spectroscopy (FTIR, Fig. 1d) and X-ray diffraction (XRD, Fig. 1e). NCF displays a strong FTIR peak at 2914 cm^{-1}, which is assigned to asymmetric stretching vibration in the pyran ring, and the peak at 3341 cm^{-1} is assigned to telescopic vibration of the O–H group. The PANI (Fig. S2) exhibits its characteristic FTIR peaks at 1493 and 1565 cm^{-1}, which are attributed to the N–B–N and N=Q=N stretching vibration, where B is benzene ring and Q stands for the quinone ring. The peak at 1306 cm^{-1} is attributed to the C–N stretching vibration. The peak corresponding to the bending external vibration of the C–H bond of the *p*-disubstituted benzene ring appears at 802 cm^{-1}. The characteristic peaks of PANI are observed in the PANI/NCF and PANI/TiO_2/NCF samples, indicating the existence of PANI in the composite samples. As an inorganic compound, TiO_2 has no characteristic peak in FTIR spectra. XRD pattern was employed to verify the existence of TiO_2. XRD spectrum of TiO_2 is shown in Fig. S3. The characteristic diffraction peaks at 25.3°, 38.0°, and 48.0° are observed in the XRD patterns of TiO_2/NCF and PANI/TiO_2/NCF samples (Fig. 1e).

Due to the addition of TiO_2 nanoparticles and the PANI nanowires, pore distribution presents a strong peak at the mesopore scale (Fig. S4), and the specific surface area increased

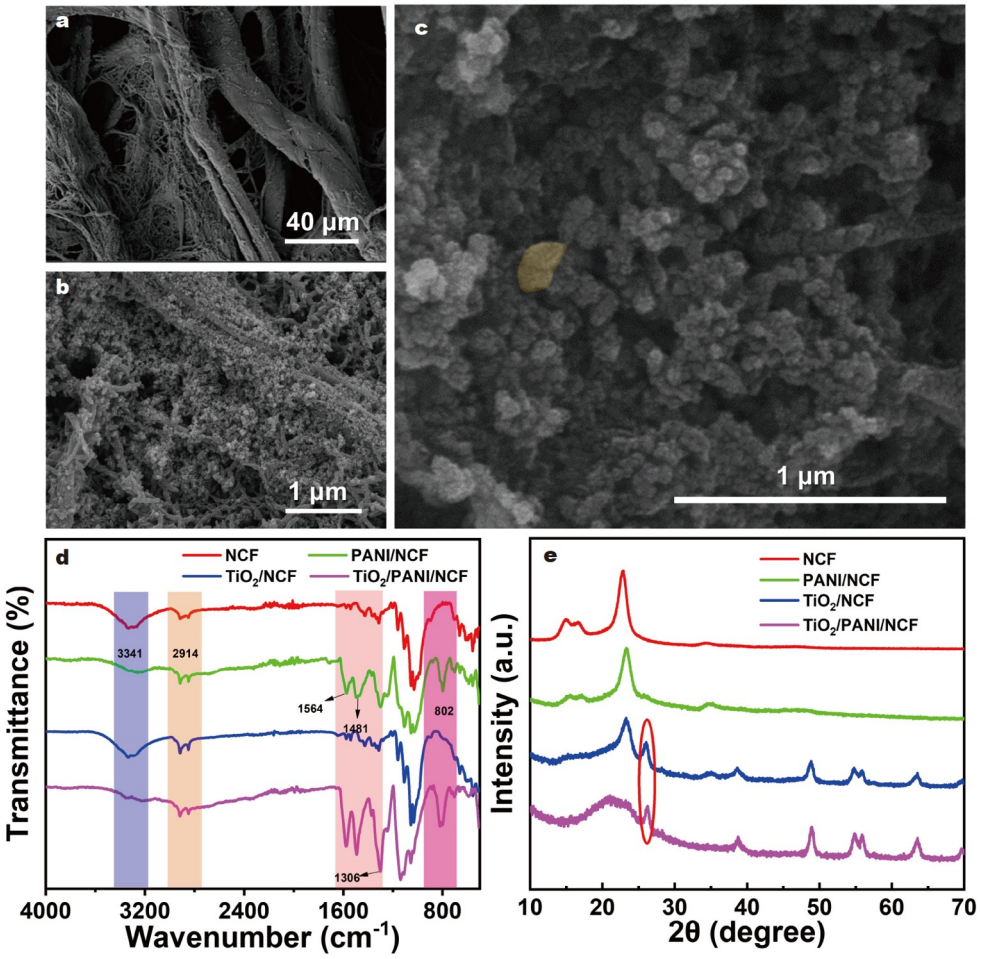

Figure 1 SEM images of (a) PANI/NCF and (b) TiO_2/PANI/NCF. (c) High-magnification SEM image of TiO_2/PANI/NCF. (d) FTIR and (e) XRD patterns of different samples (NCF, PANI/NCF, TiO_2/NCF, and PANI/TiO_2/NCF).

from 1.8 $m^2 g^{-1}$ for NCF to 9.5 and 11.8 $m^2 g^{-1}$ for TiO_2/NCF and PANI/NCF respectively. It further increases to 22.3 $m^2 g^{-1}$ for PANI/TiO_2/NCF (Table S1).

The optical property is an important factor for solar water evaporation. Fig. 2a, b present the optical transmittance and reflectance spectra of different samples. NCF displays a strong reflectance in the whole spectral range. TiO_2 is a wide-bandgap semiconductor, which shows strong absorption in the UV light region. TiO_2/NCF shows a strong light absorption in the UV region. PANI, as a conductive polymer, depicts both weak reflectance and transmittance in the full spectral range, indicating a strong absorbance over the full spectral range. Both PANI/NCF and TiO_2/PANI/NCF show low transmission and reflection in the wavelength range of 200–2500 nm, resulting in a whole solar spectrum absorption. Moreover, Fig. S5 depicts that temperature changes with light irradiation. NCF has very little temperature change. The temperature of TiO_2/NCF increases to about 50°C. The introduction of PANI makes the temperature of the PANI/NCF and PANI/TiO_2/NCF increase and maintain at a high value (70–80°C) (Fig. S5), implying that PANI is a good photothermal material. To guarantee the water supply for water evaporation, a layer of porous hydrophilic materials (suede) is replenished during the formation of the interfacial water evaporation device as shown in our previous report [44]. As shown in Fig. 2c, the photography of the water evaporation device contains the porous hydrophilic material (suede) to transport water to the PANI/TiO_2/NCF disc. The infrared thermal images were captured to characterize the wetting process of PANI/TiO_2/NCF. In the beginning, the surface of TiO_2/PANI/NCF displays a higher temperature (90.2°C) than that of the surrounding environment under light irradiation. Once water is transferred to the surface, the temperature gradually decreases and water will uniformly spread from the center to the edge. The whole disc is completely wetted after ~120 s (Fig. 2d). The prompt wetting ability is conducive to enhancing solar vapor generation. There is almost no difference in wettability between the treated sample (PANI/NCF or PANI/TiO_2/NCF) and the original sample (NCF). Furthermore, the contact angle indicates that all composites have strong water absorption (Fig. S6). As shown in Table S2, PANI fibers have high thermal conductivity, and the thermal conductivity of TiO_2/PANI/NCF is lower than that of pure PANI. Lower thermal conductivity can reduce heat loss and is conducive to solar evaporation.

Water evaporation under 1 sun simulated light

The solar water evaporation of TiO_2/PANI/NCF was optimized with different device structures. Infrared thermographies were used to monitor the surface temperature changes of different samples (pristine NCF, TiO_2/NCF, PANI/NCF, and TiO_2/PANI/NCF). The infrared images of all samples are shown in Fig. 3a (0 min row). The initial surface temperatures of all samples are 28.5–30.5°C before they are illuminated. After the light illumination for 10 min, the surface temperatures of PANI/NCF and TiO_2/PANI/NCF rapidly increase to 88.96 and 91.13°C due to the high photothermal conversion performance of PANI. The surface temperatures can only reach 41.93 and 57.6°C for the samples without PANI (NCF and TiO_2/NCF), respectively.

The increase in light absorption means converting more solar energy into heat. With an adequate water supply, the increased heat can produce more steam under the condition of continuous water supply, resulting in a higher evaporation rate. Under the same solar irradiation, the heat energy converted from the solar irradiation energy will heat the whole device. While the temperature of the device depends on the heat and water within the device [45]. Therefore, the surface temperature and water supply can be balanced by adjusting light absorbent materials and

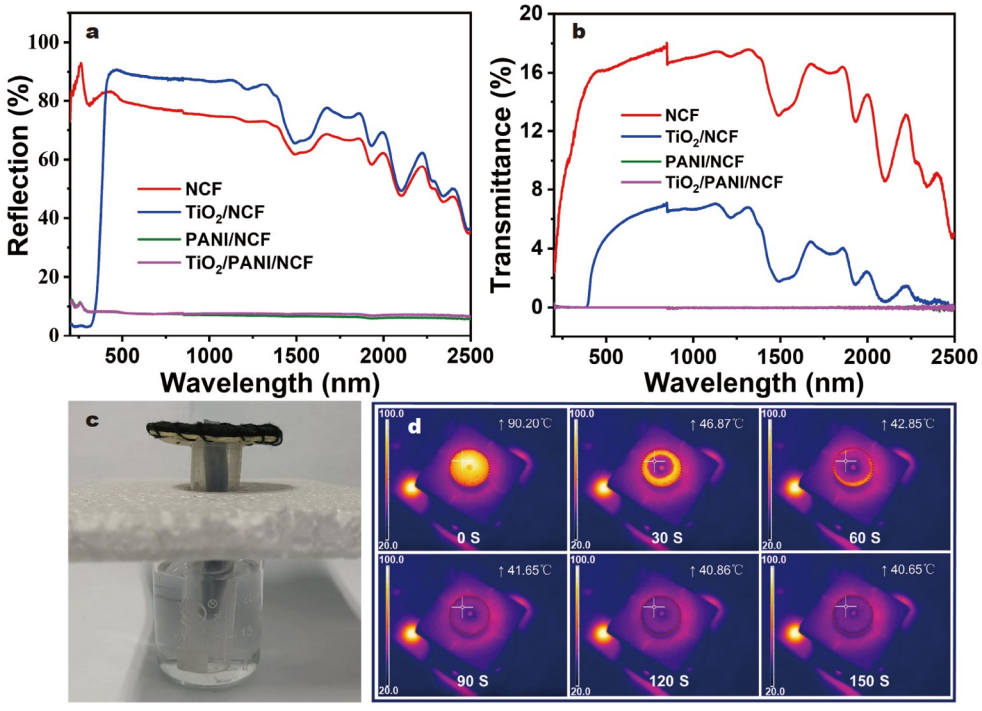

Figure 2 Reflectance (a) and transmittance (b) spectra of NCF, PANI, PANI/NCF, and TiO_2/PANI/NCF. Photograph (c) and infrared images (d) of the system for illustrating the wettability of TiO_2/PANI/NCF.

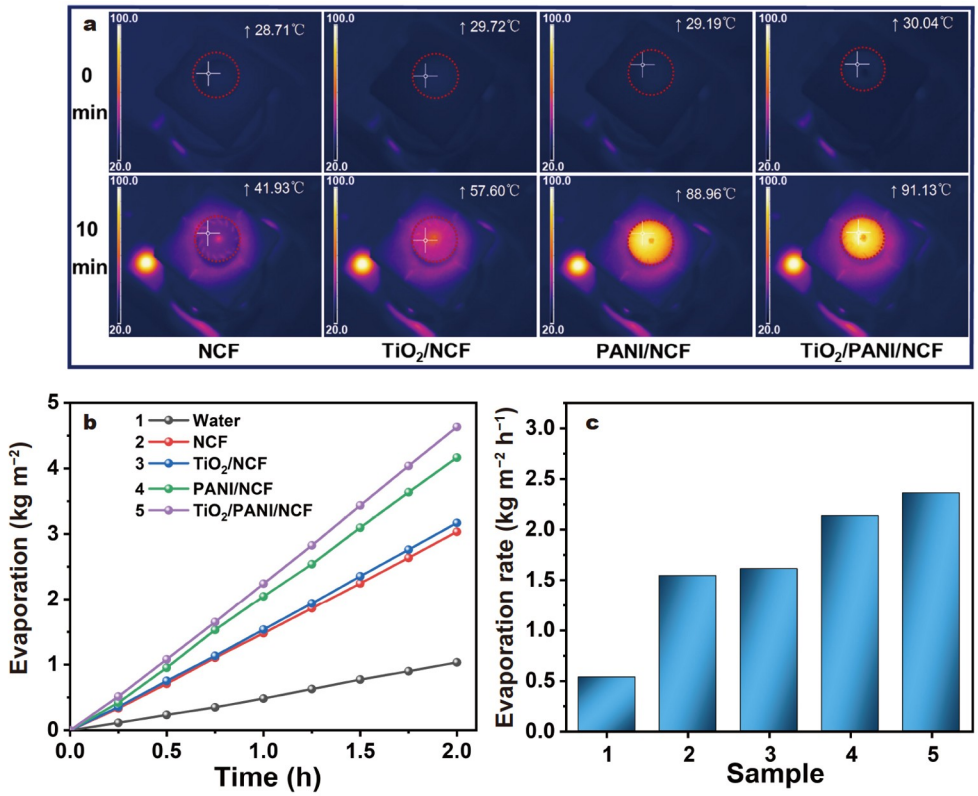

Figure 3 (a) Infrared images of NCF, PANI, PANI/NCF, TiO_2/PANI/NCF before and after 1 sun irradiation for 10 min. (b) Water evaporation quantity as a function of solar irradiation time. (c) Water evaporation rates for different samples (Sample 1: water; Sample 2: NCF; Sample 3: TiO_2/NCF; Sample 4: PANI/NCF; Sample 5: TiO_2/PANI/NCF).

device thickness to reach the optimal solar evaporation rate.

The water evaporation performance of the device was evaluated by the water evaporation rate, which was calculated from the cumulative weight of evaporated water as a function of irradiation time. To optimize the device structure, the PANI amount, device thickness, and TiO_2 amount were investigated in the PANI/TiO_2/NCF. The water evaporation rate strongly depends on the amount of photothermal materials (PANI). Therefore, the aniline amount is changed to regulate the PANI amount in the device produced with 0.32 g NCF. Fig. S7 shows that the water evaporation rate increases with the increase of the volume of aniline. When the volume of aniline is 0.4 mL, the water evaporation rate reaches 2.11 kg m^{-2} h^{-1}. The water evaporation rate does not change significantly with further increasing aniline amount. Thus, the ratio of aniline/NCF was set at 0.8 mL g^{-1}. Device thickness, as another factor, was tuned from 0.05 to 4.0 cm. As shown in Fig. S8, the average solar evaporation rate increases from 2.03 to 2.36 kg m^{-2} h^{-1} when the thickness of TiO_2/PANI/NCF increases from 0.5 to 2.0 cm. However, the evaporation rate decreases from 2.36 to ~2.26 kg m^{-2} h^{-1} when the TiO_2/PANI/NCF are thicker than 2 cm. The optimal device thickness is ~2.0 cm. Fig. 3b, c depict the water evaporation of all the device structures. NCF and TiO_2/NCF exhibit 1.5 and 1.6 kg m^{-2} h^{-1} respectively due to their porous structure. The water evaporation rate is greatly enhanced by the incorporation of PANI nanowires. The highest water evaporation rate of 2.36 kg m^{-2} h^{-1} is achieved at the optimum conditions (aniline/TiO_2/NCF = 0.4 mL/0.2 g/1.28 g and the device thickness of 2.0 cm).

Photocatalytic degradation of contaminant

Organic contaminants including herbicides, pesticides, and antibiotics cause adverse impacts on the human and environmental health. Photocatalytic degradation is an effective way to degrade them into CO_2 and H_2O. It is an ideal method to get fresh water from contaminant water by incorporating the photocatalyst into the solar water evaporator. Here, P25 TiO_2 nanoparticles as a typical photocatalyst were added to the devices. The solar water evaporation and photocatalytic degradation of TC of TiO_2/PANI/NCF under a simulated solar illumination were studied. To evaluate the degradation amount of TC, the control experiment was designed as shown in Fig. S9. To determine the TC degradation amount, we need to know how much TC (M_0) can deposit on the device over a certain evaporation time for PANI/NCF without photocatalyst. Then M_X can be obtained from the same procedure for TiO_2/PANI/NCF, which contains the photocatalyst. The difference ($M_{TC} = M_0 - M_X$) will be the amount of TC degraded by the photocatalyst. Since the device can adsorb the contaminant (TC), the device was first immersed in the 100 ppm TC solution overnight to reach saturation. We assume that the same device has the same saturated adsorption of TC. And then the device was transferred into the DI water, and the free TC would dissolve in the water. The mass of the free TC in solution (M_{B0}) can be further calculated from UV-vis spectra and the calibration curve (Fig. S10). The stock TC solution is 100 ppm and remains about 100 ppm after 10 h of water evaporation (Fig. S11), implying that the TC is transferred to the top of the device with water. TC will deposit on the device in the form of the free TC during the water eva-

poration because the devices have reached the saturated adsorption in the pretreatment. The device is transferred into the water after water evaporation. All the free TC (M_{L0}) will dissolve in the water. Then, we can calculate the deposited TC mass ($M_0 = M_{L0} - M_{B0}$) based on the adsorption peak intensity. It should be noted that part of TC might be directly degraded by light irradiation. This happens in all the water evaporation cases as well. M_0 is from the device without the photocatalyst. Similarly, the M_X can be obtained from the device with the photocatalyst (TiO_2). The photocatalytic degradation of TC can be estimated from $M_{TC} = M_0 - M_X$. The solar water evaporation experiments were carried out for 10 h under 1 simulated sunlight to reduce the measuring error. Fig. 4a presents the M_{TC} value for the device with different TiO_2 amounts. The M_{TC} value increases with the increase of the TiO_2 amount in the device. When the TiO_2 amount is over 0.8 g, M_{TC} does not increase further, implying that it reaches a balance between the degradation and TC deposition. Fig. 4b depicts water evaporation for the devices with different TiO_2 amounts, where the water evaporation rate remains at about 2.3 kg m^{-2} h^{-1}. These indicate that the PANI/TiO_2/NCF has an excellent water evaporation rate and effective organic contaminant degradation capabilities. Combining economic benefits and water evaporation degradation performance, the best effect can be achieved when the amount of TiO_2 in the device is 0.8 g.

To demonstrate the advantage of the self-cleaning solar water evaporator, TC and NaCl aqueous solutions were chosen as the contaminant water. NaCl stands for the contaminant which cannot be removed by the solar water evaporation device. As shown in Fig. 5a, when NaCl (1.0 wt%) aqueous solution is used as the stock solution, the water evaporation rate decreases greatly. The decrease in the water evaporation rate is mainly due to the accumulation of NaCl solution on the device surface. It forms solid NaCl when the NaCl concentration reaches oversaturation. The deposited NaCl will reduce the solar water evaporation performance caused by blocking light and decreasing the interface. However, using TC as the stock solution, because the TC can be quickly degraded into carbon dioxide and water, which will not cause the accumulation of pollutants and pore blockage, and thus the water evaporation rate is always maintained at a high level, which also reflects the self-cleaning ability of the bifunctional solar evaporator. Compared with the recent dual-function solar evaporator, the water evaporation rate of TiO_2/PANI/NCF presents a high-level water evaporation rate and contaminant degradation performance (Fig. 5b).

CONCLUSIONS

Photothermal PANI nanofibers are synthesized on the surface of NCF, and TiO_2 nanoparticles are added to the polymerization reaction to develop a facile solar water evaporator based on NCF. TiO_2/PANI/NCF has a wide light absorption and photocatalytic ability, which becomes a self-cleaning bifunctional solar evaporator with a high evaporation rate, and degradation of TC

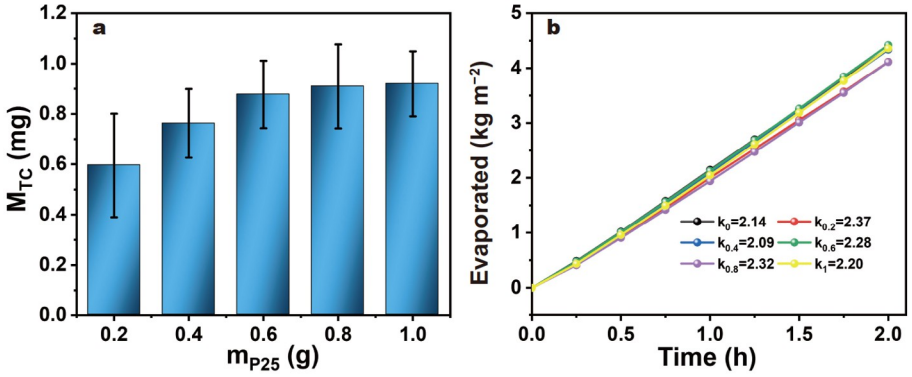

Figure 4 (a) The amount of photodegradation TC (M_{TC}) corresponds to the samples containing different amounts of P25. (b) Water evaporation rates for different samples (aniline/TiO_2/NCF = 1.6 mL/0–1 g/1.28 g).

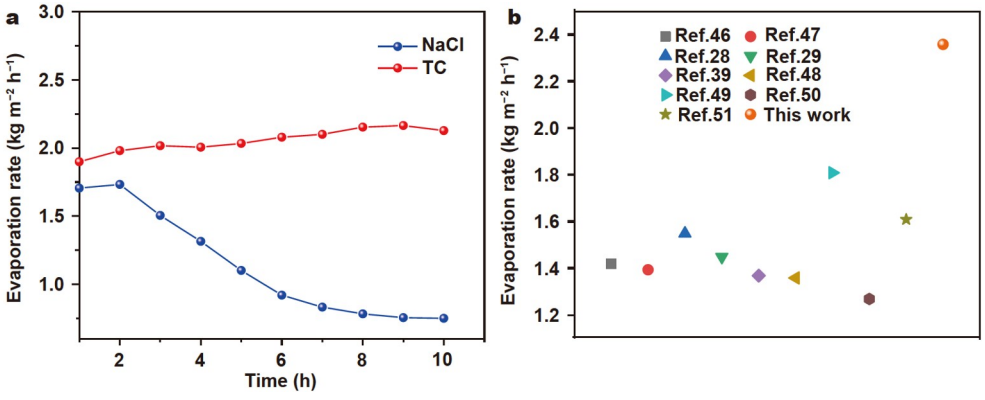

Figure 5 (a) Variation of water evaporation rate for 10 h water evaporation using the base solution of NaCl (1.0 wt%) and 100 ppm TC. (b) One-sun illumination vapor generation performance of TiO_2/PANI/NCF compared with recently reported self-cleaning solar evaporators [28,29,39,46–51].

antibiotics. The as-prepared TiO_2/PANI/NCF has a porous network structure with PANI fiber and NCF fiber interpenetrating each other, has low thermal conductivity and good hydrophilicity, and has achieved an excellent solar evaporation rate of 2.36 kg m^{-2} h^{-1} under 1 sun illumination. TiO_2/PANI/NCF makes the pollutant transfer to the surface of the solar evaporator, which is degraded rapidly and does not cause the enrichment of pollutant in the device. The solar water evaporator can maintain a high evaporation rate for a long time. TiO_2/PANI/NCF provides a novel route for water evaporation and is suitable for many different water sources, such as sewage and organic wastewater.

Received 14 September 2022; accepted 10 October 2022; published online 9 December 2022

1 Mekonnen MM, Hoekstra AY. Four billion people facing severe water scarcity. Sci Adv, 2016, 2: e1500323
2 Liu X, Zhang H, Li L, *et al.* Levels, distributions and sources of veterinary antibiotics in the sediments of the Bohai Sea in China and surrounding estuaries. Mar Pollut Bull, 2016, 109: 597–602
3 Song L, Li L, Yang S, *et al.* Sulfamethoxazole, tetracycline and oxytetracycline and related antibiotic resistance genes in a large-scale landfill, China. Sci Total Environ, 2016, 551-552: 9–15
4 Chen CQ, Zheng L, Zhou JL, *et al.* Persistence and risk of antibiotic residues and antibiotic resistance genes in major mariculture sites in southeast China. Sci Total Environ, 2017, 580: 1175–1184
5 Wang Z, Chen Q, Zhang J, *et al.* Characterization and source identification of tetracycline antibiotics in the drinking water sources of the lower Yangtze River. J Environ Manage, 2019, 244: 13–22
6 Daghrir R, Drogui P. Tetracycline antibiotics in the environment: A review. Environ Chem Lett, 2013, 11: 209–227
7 Zhu YG, Johnson TA, Su JQ, *et al.* Diverse and abundant antibiotic resistance genes in Chinese swine farms. Proc Natl Acad Sci USA, 2013, 110: 3435–3440
8 Liu H, Yang Y, Sun H, *et al.* Fate of tetracycline in enhanced biological nutrient removal process. Chemosphere, 2018, 193: 998–1003
9 Li R, Zhang L, Wang P. Rational design of nanomaterials for water treatment. Nanoscale, 2015, 7: 17167–17194
10 Gao X, Ren H, Zhou J, *et al.* Synthesis of hierarchical graphdiyne-based architecture for efficient solar steam generation. Chem Mater, 2017, 29: 5777–5781
11 Cavusoglu AH, Chen X, Gentine P, *et al.* Potential for natural evaporation as a reliable renewable energy resource. Nat Commun, 2017, 8: 617
12 Ray P. Renewable energy and sustainability. Clean Techn Environ Policy, 2019, 21: 1517–1533
13 Vishwanath Kumar P, Kumar A, Prakash O, *et al.* Solar stills system design: A review. Renew Sustain Energy Rev, 2015, 51: 153–181
14 Kabeel AE, El-Agouz SA. Review of researches and developments on solar stills. Desalination, 2011, 276: 1–12
15 Wu X, Chen GY, Owens G, *et al.* Photothermal materials: A key platform enabling highly efficient water evaporation driven by solar energy. Mater Today Energy, 2019, 12: 277–296
16 Deng Z, Zhou J, Miao L, *et al.* The emergence of solar thermal utilization: Solar-driven steam generation. J Mater Chem A, 2017, 5: 7691–7709
17 Ni G, Li G, Boriskina SV, *et al.* Steam generation under one sun enabled by a floating structure with thermal concentration. Nat Energy, 2016, 1: 16126
18 Ghasemi H, Ni G, Marconnet AM, *et al.* Solar steam generation by heat localization. Nat Commun, 2014, 5: 4449
19 Jiang Q, Tian L, Liu KK, *et al.* Bilayered biofoam for highly efficient solar steam generation. Adv Mater, 2016, 28: 9400–9407
20 Hao L, Liu N, Niu R, *et al.* High-performance salt-resistant solar interfacial evaporation by flexible robust porous carbon/pulp fiber membrane. Sci China Mater, 2022, 65: 201–212
21 Li Y, Jin X, Li W, *et al.* Biomimetic hydrophilic foam with micro/nanoscale porous hydrophobic surface for highly efficient solar-driven vapor generation. Sci China Mater, 2022, 65: 1057–1067
22 Guo D, Yang X. Highly efficient solar steam generation of low cost TiN/bio-carbon foam. Sci China Mater, 2019, 62: 711–718
23 Zhu HW, Ge J, Zhao HY, *et al.* Sponge-templating synthesis of sandwich-like reduced graphene oxide nanoplates with confined gold nanoparticles and their enhanced stability for solar evaporation. Sci China Mater, 2020, 63: 1957–1965
24 Zhu M, Li Y, Chen F, *et al.* Plasmonic wood for high-efficiency solar steam generation. Adv Energy Mater, 2018, 8: 1701028
25 Chen M, He Y, Huang J, *et al.* Synthesis and solar photo-thermal conversion of Au, Ag, and Au-Ag blended plasmonic nanoparticles. Energy Convers Manage, 2016, 127: 293–300
26 Gao T, Wang Y, Wu X, *et al.* More from less: Improving solar steam generation by selectively removing a portion of evaporation surface. Sci Bull, 2022, 67: 1572–1580
27 Wang Y, Wu X, Wu P, *et al.* Enhancing solar steam generation using a highly thermally conductive evaporator support. Sci Bull, 2021, 66: 2479–2488
28 Xing J, Tong J, Liu Y, *et al.* A high-efficiency ammonia-responsive solar evaporator. Nanoscale, 2020, 12: 9680–9687
29 Hao D, Yang Y, Xu B, *et al.* Bifunctional fabric with photothermal effect and photocatalysis for highly efficient clean water generation. ACS Sustain Chem Eng, 2018, 6: 10789–10797
30 Zhao X, He Z, Ou W, *et al.* Narrow-bandgap light-absorbing conjugated polybenzobisthiazole: Massive interfacial synthesis, robust solar-thermal evaporation and thermoelectric power generation. Sci China Mater, 2022, 65: 2491–2501
31 Yin Q, Zhang J, Tao Y, *et al.* The emerging development of solar evaporators in materials and structures. Chemosphere, 2022, 289: 133210
32 Zhang L, Tang B, Wu J, *et al.* Hydrophobic light-to-heat conversion membranes with self-healing ability for interfacial solar heating. Adv Mater, 2015, 27: 4889–4894
33 Jiang Q, Gholami Derami H, Ghim D, *et al.* Polydopamine-filled bacterial nanocellulose as a biodegradable interfacial photothermal evaporator for highly efficient solar steam generation. J Mater Chem A, 2017, 5: 18397–18402
34 Chen Q, Pei Z, Xu Y, *et al.* A durable monolithic polymer foam for efficient solar steam generation. Chem Sci, 2018, 9: 623–628
35 Chen C, Kuang Y, Hu L. Challenges and opportunities for solar evaporation. Joule, 2019, 3: 683–718
36 Yang Y, Zheng Z, Yang M, *et al.* *In-situ* fabrication of a spherical-shaped Zn-Al hydrotalcite with BiOCl and study on its enhanced photocatalytic mechanism for perfluorooctanoic acid removal performed with a response surface methodology. J Hazard Mater, 2020, 399: 123070
37 Park J. Visible and near infrared light active photocatalysis based on conjugated polymers. J Ind Eng Chem, 2017, 51: 27–43
38 Tahir M. Well-designed $ZnFe_2O_4$/Ag/TiO_2 nanorods heterojunction with Ag as electron mediator for photocatalytic CO_2 reduction to fuels under UV/visible light. J CO_2 Util, 2020, 37: 134–146
39 Li R, Zhou C, Yang L, *et al.* Multifunctional cotton with PANI-Ag NPS heterojunction for solar-driven water evaporation. J Hazard Mater, 2022, 424: 127367
40 Li S, He Y, Wang Y, *et al.* Simple hierarchical interface design strategy for accelerating solar evaporation. Macromol Mater Eng, 2021, 306: 2000640
41 Huang J, Virji S, Weiller BH, *et al.* Polyaniline nanofibers: Facile synthesis and chemical sensors. J Am Chem Soc, 2003, 125: 314–315
42 Mo Z, Zhao Z, Chen H, *et al.* Heterogeneous preparation of cellulose-polyaniline conductive composites with cellulose activated by acids and its electrical properties. Carbohydr Polym, 2009, 75: 660–664
43 Cao S, Rathi P, Wu X, *et al.* Cellulose nanomaterials in interfacial evaporators for desalination: A "natural" choice. Adv Mater, 2021, 33: 2000922
44 Sun Y, Zong X, Qu D, *et al.* Water management by hierarchical structures for highly efficient solar water evaporation. J Mater Chem A,

2021, 9: 7122–7128
45 Gong F, Wang W, Li H, *et al.* Solid waste and graphite derived solar steam generator for highly-efficient and cost-effective water purification. Appl Energy, 2020, 261: 114410
46 Xu Y, Ma J, Han Y, *et al.* Multifunctional CuO nanowire mesh for highly efficient solar evaporation and water purification. ACS Sustain Chem Eng, 2019, 7: 5476–5485
47 Li J, Jing Y, Zhou X, *et al.* Multifunctional photothermal materials based on natural pumices for high efficiency solar-driven interface evaporator. Int J Energy Res, 2021, 45: 20132–20142
48 Lu Y, Wang X, Fan D, *et al.* Biomass derived Janus solar evaporator for synergic water evaporation and purification. Sustain Mater Technol, 2020, 25: e00180
49 Wu P, Wu X, Wang Y, *et al.* Boosting extraction of Pb in contaminated soil *via* interfacial solar evaporation of multifunctional sponge. Green Energy Environ, 2022, :
50 Ming X, Guo A, Zhang Q, *et al.* 3D macroscopic graphene oxide/MXene architectures for multifunctional water purification. Carbon, 2020, 167: 285–295
51 Geng X, Zhang D, Zheng Z, *et al.* Integrated multifunctional device based on Bi_2S_3/Pd: Localized heat channeling for efficient photothermic vaporization and real-time health monitoring. Nano Energy, 2021, 82: 105700

Acknowledgements This work was supported by the National Natural Science Foundation of China (21872001, 51801006, 21805004, and 21671011), Beijing Municipal High Level Innovative Team Building Program (IDHT20180504), Beijing Outstanding Young Scientists Program (BJJWZYJH01201910005017), Beijing Natural Science Foundation (2192005), and Beijing Municipal Science and Natural Science Fund Project (KM201910005016).

Author contributions Liu W and Sun Z designed the experiment. Liu W prepared the samples and performed the measurement and characterization with most of the analysis. All authors contributed to the discussion of the results. Liu W and Sun Z led the effort in the writing of the manuscript.

Conflict of interest The authors declare that they have no conflict of interest.

Supplementary information Experimental details and supporting data are available in the online version of the paper.

Wenning Liu is a PhD student at Beijing Key Laboratory for Green Catalysis and Separation, Department of Chemistry and Chemical Engineering, Beijing University of Technology. Her current research interests focus on polymer-based solar evaporation devices.

Zaicheng Sun received his PhD degree in chemistry from Changchun Institute of Applied Chemistry, Chinese Academy of Sciences (CAS). After that, he started to work as an AvH research fellow at Marburg University in Germany, followed by research associate at UW, UDel, and UNM. He took the professor position at Changchun Institute of Optics, Fine Mechanics and Physics, CAS in 2010. He is currently a professor at the Department of Chemistry and Biology, Beijing University of Technology. His research focuses on the rational design of photocatalysts with high charge separation efficiency and fluorescent carbon dots with tunable emission and their applications.

基于聚苯胺/二氧化钛/天然纤维素的污水自清洁太阳能水蒸发装置

刘文宁, 李鹏飞, 李湘勤, 何亚倩, 安丽, 曲丹, 汪夏燕, 孙再成*

摘要 水体污染是当前造成淡水短缺的主要原因之一. 利用太阳能水蒸发装置从海水或污水中生产淡水是一种简单有效且节能的解决淡水危机的方式, 引起了广泛的关注. 然而, 污染物的共同蒸发或沉积可能会降低水蒸发过程中的效率和淡水质量. 本文基于天然木质纤维素(NCF)、聚苯胺(PANI)和二氧化钛(TiO_2)开发了自清洁太阳能水蒸发器, 其具有宽吸收、亲水性强、导热系数低等优点. 通过在聚合物溶液中加入木质纤维素, 聚苯胺纳米纤维在NCF表面聚合形成介孔网络. P25 TiO_2纳米颗粒作为光催化剂分散到上述反应液中, 通过简单的过滤形成PANI/TiO_2/NCF复合材料. 由于太阳水蒸发器装置中PANI的光热效应与TiO_2纳米颗粒的光催化降解的协同作用, 水蒸发速率可达2.36 kg m^{-2} h^{-1} (1个太阳光照射下), 且可有效降解污染物(100 ppm四环素). 更重要的是, 在工作10 h后, 该太阳能水蒸发器装置仍然保持稳定的水蒸发速率, 且没有污染物的积聚. 光催化和光热效应相结合的双功能太阳能水蒸发装置在有机污染物水中具有自清洁作用, 具有很大的应用潜力.

